Scientific Report

Regarding the Project Implementation during January - December 2014

Phase IV. The realization of the experimental model of magnetic doped TiO_2 nanoparticles embedded in siloxane polymer: results obtained at different Ti doping levels (low/ high fluxes of Ti gas precursor).

1. Synthesis by laser pyrolysis of nanosized magnetic nanoparticles (maghemite iron oxide core) embedded in carbosilane polymer (HMDSO as precursor) doped with TiO_2 at low/ high Ti doping levels.

2. UV-Vis, XRD, TEM, SEM analyses

3. Magnetic characterization

4. Photocatalytic activity of TiO_2-based nanopowders

Introduction

In the process of photocatalysis, TiO_2 is considered almost ideal semiconductor and is used in photodegradation processes of organic compounds due to: higher specific surface area, efficient absorption of light, good dispersion [1-3]. By the introduction of iron into the structure of TiO_2 the new magnetic composite obtained can be separated / collected from the water by applying an external magnetic field. In this regard, nanoparticles type core-shell in which the core is magnetite and the shell is TiO_2 are reported in the most studies because are considered to be inexpensive and non-toxic materials [4-7]. Also, recent studies have shown that the photocatalytic efficiency of TiO_2 has decreased by introducing magnetic core, and was thus necessary the introduction of an additional inert shell between the magnetic core and TiO_2 acting like a buffer to prevent the photodissolution of magnetic core [8] and the transfer of electrons-holes from TiO_2 to core particle. This shell can be a passive SiO_2 which can contribute to improved stability and dispersibility of the magnetic core in corrosive solutions All nanocomposites obtained in the above studies have been synthesized following the multi-stage synthesis [9-11].

In this stage, the magnetic TiO_2 nanocomposites coated / embedded in SiO_2 shell/matrix was obtained in a single step method using laser oxidative pyrolysis.

1. Synthesis by laser pyrolysis of nanosized magnetic nanoparticles (maghemite iron oxide core) embedded in carbosilane polymer (HMDSO as precursor) doped with TiO_2 at low/ high Ti doping levels.

Magnetic titania nanoparticles covered/embedded in SiO_2 shell/matrix was obtained using laser pyrolysis as method synthesis. The method was described in detail in our previous stages; in this case the experimental setup was modified by changing the gases inlet system in the reaction chamber. Considering the flow of precursors and the diameter of laser beam was developed a new system consisting of three concentric nozzles controlling thus the reaction zone. The entry of precursors in the reaction chamber was established to not react chemically before encountering laser radiation as presented in Fig.1 following the parameteres summarized in Table 1.

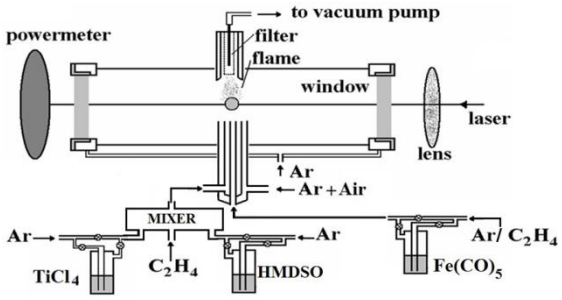

Fig. 1. Experimental setup for the synthesis of titania based nanocomposites by laser pyrolysis

The choice of such geometries was aimed at the formation of Fe^{3+} metal core coated with TiO_2 and SiO_2 to provide improved magnetic properties compared with those of TiO_2. The first step aimed at obtaining pure TiO_2 nanopowders with anatase majority phase for a good applications in photocatalysis process (sample T). In the second stage the introduction of Fe in TiO_2 lattice for magnetic properties by the addition of Fe $(CO)_5$ flow of vapour carried by an inert gas Ar was aimed (sample named TF). The third stage was aimed to improve stability and dispersability of TiO_2 nanoparticles by introducing a carrier gas of different nature through the HMDSO bubbler (for TFS-1 inert Ar and for TFS-2 C_2H_4).

Table 1. Experimental parameters and EDS measurements for the TiO_2 based samples [a]

Sample	$\Phi_{Ar\,sheat}$ [sccm]	ΦAir [sccm]	$\Phi_{Ar,}$ $TiCl_4$ [sccm]	ΦC_2H_4 [sccm]	Φ_{Ar} › HMDSO [sccm]	$\Phi_{Ar,}$ $Fe(CO)_5$ [sccm	Φ C_2H_4, $Fe(CO)_5$ [sccm]	P [mbar]	Yield [g/h]	EDAX (at%)				
										Fe	Ti	O	Si	C
T	600	1400	200	30	0	0	0	450	1.05	0	29.07	64.80	0	6.13
TF	600	1400	200	30	0	**10**	0	450	1.03	1.67	31.51	56.87	0	9.95
TFS-1	600	1400	200	30	**20**	10	0	450	1.92	1.68	16.53	61.09	12.36	8.34
TFS-2	600	1400	200	30	20	0	**10**	450	2.25	1.92	13.69	57.10	13.70	13.59

[a] The following parameters were maintained constant: the flows of Ar for windows flushing (ΦAr_{window} = 1750 sccm), the total pressure (P_{mbar} = 450) and the laser power (P_{watt} = 400).

2. UV-Vis, XRD, TEM, SEM analyses

EDX measurements

In the Table 1 are presented the experimental parameters and the the results of EDX semi quantitative elemental analysis for all the samples. The results of the analyzes indicate a good correlation between the gas flows and Si content, and because the introduction of $Fe(CO)_5$ is made using ethylene in the sample TFS-2 (as compare with TFS-1), its growth is also correlated with increasing carbon and iron content. The iron amount in TiO_2 samples increases because in the laser pyrolysis process the ethylene played role as sensitizer and by introduction in intimate mixture with iron precursor leads to the its decomposition and indirectly for the others reactant precursors.

XRD analysis

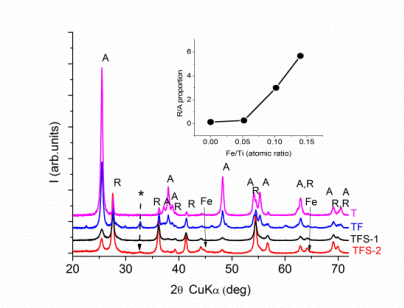

Fig. 2. XRD diffraction patterns for the samples T, TF, TFS-1and TFS-2 with anatase (A) rutile (R), iron (Fe) and α-Fe_2O_3 peak identification.

The XRD diffraction patterns (Fig.2) of all raw samples show a mixture of TiO_2 phases anatase (JCPDS file 21-1272) and rutile (JCPDS file 21-1276). The manifest trend of the effect of Fe doping is the preponderance of the rutile phase. The evolution of proportion of the anatase and rutile phases evaluated according to empiric formula of Spurr and Myers [12] shows an almost linear increase with the Fe/Ti atomic ratio estimated via EDAX (inset in Fig XRD). In the sample with the highest amount of Fe (TFS-2) peaks of metallic Fe (JCPDS file 06-0696) are observed. The result is consistent with the Mossbauer analysis. Weak Fe peaks are also observable, in particular in the TFS-1 XRD pattern. A common peak is presented in all the Fe containing samples which is clearly visible in TFS-1. It can tentatively be assigned to an α-Fe_2O_3 phase (JCPDS file 39-0238). The existence of amorphous it is also to be considered, in particular in the HMDSO derived syntheses. The mean crystallite sizes

estimated by the Scherrer formula, using the most intense maxima of the two TiO2 phases are included in table 2. The effect of Fe doping is the decrease of crystallite dimensions.

Table 2. Crystallographic parameters estimated from XRD measurements for the TiO_2 based nanocomposites.

Sample	TiO_2 phases (R = rutile, A = anatase)		
	R/A proportion	D_A (nm)	D_R(nm)
T	0.14	22	34
TF	0.27	18	24
TFS-1	3.00	10	17
TFS-2	5.67	14	20

TEM analysis

Higher magnification TEM micrographs for samples exhibit both round shaped and elongated or facetted particles, with irregular shapes and sizes (Fig. 3a-c, for samples T, TF and TFS-1). For the sample TFS-1 the morphology consisting of core–shell particles, with various thicknesses of the shells or amorphous carbon/SiO_2 matrix are reveals. The associated SAED patterns in which the formation of different phase in the synthesized nanocomposites was also analyzed and presented as insets in Fig. 3a-c. The major anatase presence ((101), (200), (105) and (204)) are presented in the sample T (pure TiO_2) while rutile phase is evidenced in samples containing iron by reduced FFT of TFS-1sample (inset Fig.3c).

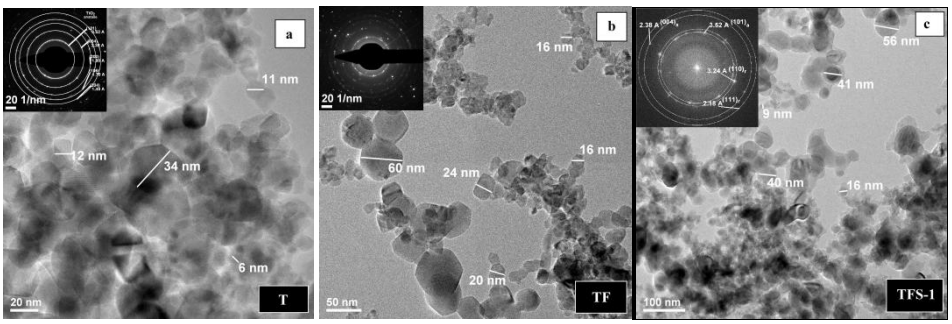

Fig. 3. TEM images of the TiO_2 based nanocomposites and the corresponding SAED or FFT patterns (as inset in figures): a - for the TiO_2 sample (T); b-for the Fe- TiO_2 sample (TF) and c — for sample Fe-TiO_2 covered/embedded in SiO2 shell/matrix .

Fig. 4 displays the HRTEM images for sample: TF (a, c) and TFS-1(b). A mixture of anatase and rutile (d=3.52 and 3.24 Å interplanar distances, respectively) with α-Fe_2O_3 (d=3.7) surrounded/embedded by amorphous SiO_2 seems to be present in sample- obtaining a good correlation with SAED and XRD analyses.

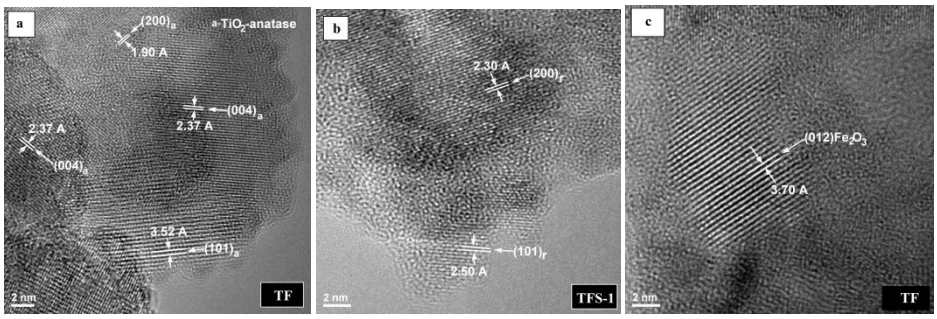

Fig. 4. HRTEM images showing interplanar spacings which may correspond to: a -anatase (101), (004), (200); b – rutile (101), (200) and c – α-Fe_2O_3 (110) and (023)

Characterization by UV-Vis transmission spectroscopy

The optical properties of titania based nonocomposites were investigated by measuring their band-gap energy (Eg). This value reported in the literature is 3.2 eV for anatase phase of TiO_2. The UV-Vis absorption edge and band gap energies of the samples have been determined from the reflectance [F(R)] spectra using the K-M (Kubelka–Munk) formalism [13,14] and the Tauc plot for the synthesized TiO_2 based samples. By the extrapolation lines shown in Fig. 5 have been used to determine the band gaps for three different kind of samples: pure-TiO_2 (sample T), magnetic-TiO_2 (sample TF) and magnetic TiO_2 nanoparticles covered/embedded in SiO_2 shell/matrix (sample TFS-1).

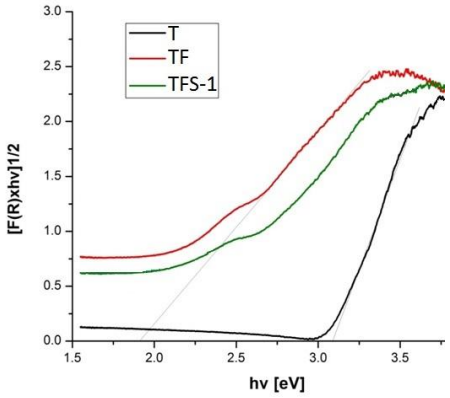

Fig. 5. Absorbance spectra for the indirect electronic transition $F(R)^{1/2}$ vs E (eV) for the sample T (TiO_2 free iron), TF (TiO_2 with iron) and TFS-1 (TiO_2 with iron and polimer)

3. Magnetic characterization

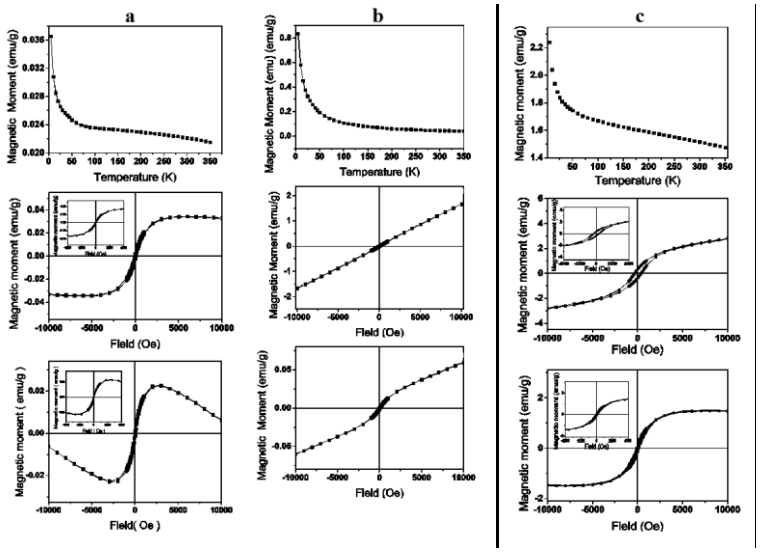

Fig. 6. FC-ZFC and Hysteresis magnetization curves for T (a), TF (b) and TFS-2 (c) samples

Very low temperature Mossbauer spectra (at 5 K) of TF and TFS-1 presents a superposition of doublets (from (super)paramagnetic phases) and sextets (from magnetic blocked/ordered phases) that can be ascribable to Fe oxide clusters highly dispersed in/impurified with TiO_2 for TF or TiO_2 and SiO_2 for TFS-1, the TFS-1cluster mean size (containing 95% Fe^{3+} and 5% Fe^{2+}) being smaller as compared with those from TF (with Mossbauer blocking temperature ~ 20 K); also, in the TFS-1sample, the amount of Fe^{3+} completely dispersed ions is greater than those from TF powder. A completely paramagnetic behavior can be seen at 60 K for TF sample. The hyperfine field values associated with the three sextets from TF sample vary between 46 to 40 T, ascribable to very small and defective clusters (~2-3 nm) of Fe oxides highly impurified with Ti ions. The reference sample without Fe content (or any other magnetic traditional elements) - *T* - show a very low saturation magnetization (~ 3.4 x 10^{-2} emu/g at 5 K with B> 0.5 T) which can be associated to defects of TiO_2 matrix, presenting thus a diluted magnetic oxide (DMO) behavior. The signal is weaker at RT (300 K) due to oxide diamagnetism. After substraction of the diamagnetic component, the long-range ordered component appears that has a coercive field of ~ 100 Oe at 5K and 30 Oe at RT, confirmed also by temperature-magnetization curve. At least two magnetic components can be extracted from RT hysteresis curve of the TF (Fe-containing) sample. Corroborated with Mossbauer spectra, the ferromagnetic component in this sample can be associated again with TiO_2 matrix and the paramagnetic component with Fe^{3+} ions. The lacking of saturation of magnetization at 5 K for this sample is related with the very defective cluster structure and the

predominance of magnetic signal from Fe. Again, from RT hysteresis curve, after the substraction of the superparamagnetic component, the resulted ordered magnetic component saturation magnetization is ~ 3.5 x 10^{-2} emu/g (very near to corresponding Ms value T sample at 5 K). TFS-1sample shows a very similar behavior whit those of TF sample. The sample TFS-2 shows a consistent RT magnetization (approx 1.5 emu / g, approximately an order of magnitude higher than previous samples). At low temperatures is observed a superposition of paramagnetic contributions and a magnetically ordered (saturation magnetization and coercive field) magnetic component having a saturation magnetization of the same order 1.5 emu/g. Coercive field is about 350 Oe at 5 K and 115 Oe at RT therefore higher values than those observed in previous samples. Mossbauer spectra reveals a phase with hyperfine ~30 T isomer shift which can be associated only to metallic strongly impurified Fe phases. The contribution of this phase decreases from 27% to 5 K, from 15% to 30 K, and then remains approximately constant (it remains stationary at about 29T), suggesting the formation of iron NP with high blocking temperature (probably above RT).

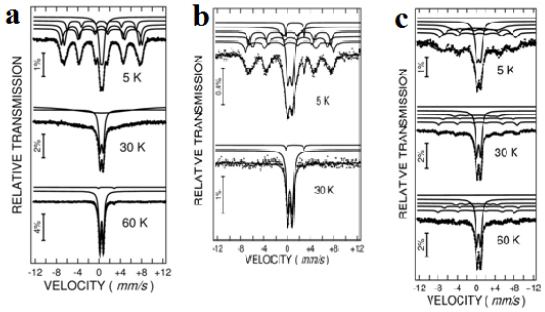

Fig.7 Low temperatures Mossbauer spectra for (a)TF,(b)TFS-1 and (c) TFS-2 nanocomposites

4. Photocatalytic activity of TiO_2-based nanopowders

The presented results from Table 3 reveal that all the samples have lower band gap energy than the TiO_2 Degussa commercial sample (3.2 eV) and the greatest reduction in the band gap (E_g= 1.85 eV) is observed for magnetic-TiO_2 sample (TF). These redshifting of light absorption of our samples is promising for a better photocatalytic efficiency as visible-light-active photocatalyst.

3. The energy values of the indirect bandgap transitions for the synthesized TiO_2 based nanocomposites

Sample	**Bandgap energy (eV)** for **Indirect transition type**

T	**3.08**
TF	**1.85**
TFS-1	**2.22**

Conclusions

Magnetic- $TiO_2@SiO_2$ nanoparticles were successfully synthesized by the laser pyrolysis method; this technique offers the advantage of using a single-step gas-phase doping/covering method. Resulted nanopowders contain mixtures of anatase and rutile phases, with mean crystallite dimensions (in the 14-34 nm range) and good crystallinity. Magnetic analysis reveals that the Fe-doped TiO_2-based samples present a typical character of diluted magnetic oxide systems. Iron-doped $TiO_2@SiO_2$ samples have a lower bandgap energy than the TiO_2 P25 Degussa sample (Eg= 1.85 eV for the sample TF).

References

[1] K. W. Kim, S. H. You, S. S. Park,G.H.Kang, W. T. Bae, andD. W. Shin, "Effect of experimental conditions on photocatalytic efficiency in TiO 2 powder slurry systems," Journal of Ceramic Processing Research, vol. 9, no. 5, 530–537, 2008.

[2] I. Arslan, I. A. Balcioglu, and D. W. Bahnemann, "Heterogeneous photocatalytic treatment of simulated dyehouse effluents using novel TiO2-photocatalysts," Applied Catalysis B, vol. 26, no. 3, 193–206, 2000.

[3] N. Bouanimba, R. Zouaghi, N. Laid, and T. Sehili, "Factors influencing the photocatalytic decolorization of Bromophenol blue in aqueous solution with different types of TiO2 as photocatalysts," Desalination, vol. 275, no. 1–3, 224–230,2011.

[4] D. Beydoun, R. Amal, G. K. C. Low, and S. McEvoy, "Novel photocatalyst: titania-coated magnetite. Activity and no. 18, 4387–4396, 2000.

[5] D. Beydoun, R. Amal, J. Scott, G. Low, and S.McEvoy, "Studies on themineralization and separation efficiencies of amagnetic photocatalyst," Chemical Engineering & Technology, vol. 24, no. 7, 745–748, 2001.

[6] F. Chen, Y. Xie, J. Zhao, and G. Lu, "Photocatalytic degradation of dyes on a magnetically separated photocatalyst under visible and UV irradiation," Chemosphere, vol. 44, no. 5, 1159–1168, 2001.

[7] D. Beydoun and R. Amal, "Implications of heat treatment on the properties of a magnetic iron oxide-titanium dioxide photocatalyst," Materials Science and Engineering B, vol. 94, no. 1, 71–81, 2002.

[8] D. Beydoun, G. Low , S. McEvoy, Occurrence and prevention of photodissolution at the phase junction of magnetite and titanium dioxide, J. Molec. Catal. A 180, pp.193-200, 2002

[9] D. Bydoun, R. Amal, G. Low, S. McEvoy, Influence of plasma spraying parameter on microstructure and hotocatalytic properties of nanostructured TiO2–Fe3O4 coating, J. Mol. Catal. A: Chem. 283, 23–28,2008.

[10] D. Beydoun, R. Amal, G.K.-C. Low, S. McEvoy, Novel photocatalysts: titaniacoated magnetite. Activity and photodissolution, J. Phys. Chem. B 104 387–4396, 2000

[11] D.G. Shchukin, A.I. Kulak, D.V. Sviridov, Magnetic photocatalysts of core–shell type, Photochem. Photobiol. Sci. 1 742–744, 2002

[12] R.A Spurr, H. Myers, Quantitative analysis of anatase-rutile mixtures with an X-Ray diffractometer, Anal. Chem. 29, 760,1957.

[13] S. Valencia, J. M. Marín, G. Restrepo, Study of the bandgap of synthesized titanium dioxide nanoparticules using the sol-gel method and a hydrothermal treatment, The Open Materials Science Journal 4 (2010) 9-14.

[14] S.Tandon, J. Gupta, Measurement of forbidden energy gap of semiconductors by diffuse reflectance technique, Phys Stat Sol 38 (1970) 363-7.

Dissemination

International Conference presentation:

1. C. Fleaca**,** M. Scarisoreanu, I. Morjan, C. Luculescu, A.-M. Niculescu, F. Dumitrache, .E. Vasile, V. Danciu, M. Popa "**One-step laser pyrolysis synthesis of TiO_2 nanoparticles embedded in carbon-silica shells/matrix**˝ E-MRS Spring Meeting, Lille, France, May 26-30, 2014

2. M. Scarisoreanu, I. Morjan., C.-T. Fleaca, I.P. Morjan, A-M..Niculescu, E. Dutu, A.Badoi, R. Birjega, C. Luculescu, E. Vasile, V. Danciu, G. Filoti "**Synthesis and photocatalytic properties of novel multifunctional TiO_2-based magnetic nanocomposite**'' E-MRS Spring Meeting, Lille, France, May 26-30, 2014

Scientific publication:

1. C.T. Fleaca, M. Scarisoreanu, I. Morjan, C. Luculescu, A.-M. Niculescu, A. Badoi, E. Vasile, G. Kovacs "**Laser oxidative pyrolysis synthesis and annealing of TiO_2 nanoparticles embedded in carbon-silica shells/matrix**" - accepted for publication

2. M. Scarisoreanu, C.-T. Fleaca, , I. Morjan., I.P. Morjan, A-M..Niculescu, E. Dutu, A.Badoi, R. Birjega, C. Luculescu, E. Vasile, V. Danciu, G. Filoti "**Synthesis and photocatalytic properties of novel multifunctional TiO_2-based magnetic nanocomposite** - under revision

Project Director,

Dr. Claudiu Fleaca